COMMUNICATIONS IN SCIENCE AND TECHNOLOGY
Homepage: cst.kipmi.or.id

Physico-chemical characteristics of Ca/P ratio on the composition and structure of oxygenated apatite

S. Jerdioui[a], H. Bouammali[a], E. Mejdoubi[a], R. Touzani[a], K. Azzaoui[b,c], B. Hammouti[c,d], R. Sabbahi[e], Asep Bayu Dani Nandiyanto[f,*], L. L. Elansari[a]

[a]*Laboratory of Applied Chemistry and Environment (LCAE), Department of Chemistry, University Mohamed I, Oujda 60000, Morocco*
[b]*Engineering Laboratory of Organometallic, Molecular Materials and Environment, Sidi Mohammed Ben Abdellah University, Fez 30000, Morocco*
[c]*Euromed University of Fes, UEMF, Fes 30000, Morocco*
[d]*Laboratory of Industrial Engineering, Energy and the Environment (LI3E) SUPMTI, Rabat, Morocco*
[e]*Research team in Science and Technology, Higher School of Technology, Ibn Zohr University, Laayoune 3007, Morocco*
[f]*Universitas Pendidikan Indonesia, Bandung, Indonesia*

Article history:
Received: 29 January 2024 / Received in revised form: 14 June 2024 / Accepted: 15 June 2024

Abstract

Phosphocalcic apatites have osteoconductive and bioactive properties that make them suitable for bone reconstruction. But, they are inactive against pathogenic microorganisms that can infect bone tissue. To overcome this limitation, we synthesized oxygen-doped phosphocalcic apatites that can release molecular oxygen as a bioactive molecule. We investigated how the calcium-to-phosphorus ratio (Ca/P) gave impacts on the chemical and structural composition of the oxygen-doped phosphocalcic apatites. We here used the double decomposition method, which involved mixing calcium nitrate and diammonium phosphate solutions in an ammonia buffer. We then characterized the products using several analysis, including infrared absorption spectroscopy, X-ray diffraction, thermal analysis, nitrogen adsorption-desorption, and elemental chemical analysis. It was found that the oxygen-doped phosphocalcic apatites were calcium-deficient and had a well-defined crystallinity at room temperature. After calcination at 900°C, the crystallinity improved further. The thermal analysis showed two mass losses: one at 50°C due to water adsorption and another at 450°C due to CO_2 release. The specific surface area was about 100 ± 2 m^2/g without any change with the Ca/P ratio. The quantity of molecular oxygen increased with the Ca/P ratio and reached an optimal value of the order of 3.6 $\times 10^{-4}$ mol for Ca/P=1/65 with the chemical formula of $Ca_{9.9}(PO_4)_6(OH)_{1.25}(O_2)_{0.74}(CO_3)_{0.01}$. It is important to make further analysis to know more about the properties of oxygenated apatite, and to combine this apatite with polymers purposely to have biomedical composites. It then can be concluded that the oxygen-doped phosphocalcic apatites could be a promising biomaterial for bone infection prevention and treatment. This research highlights an oxygenation treatment of phosphocalcic apatite and brings new ideas and possibilities for future research and development to get better understanding of the behavior of these biomaterials to be more effective, especially in the biological field. As a perspective, improving the biological properties in these biomaterials needs to be further explored, including experimental parameters for the obtainment of more conclusive results.

Keywords: antiseptic; biomaterials; double decomposition; oxygenated apatite; phosphate

1. Introduction

Hydroxyapatite (HAp) is a mineral that resembles the composition and structure of the calcified tissues in bones and teeth [1-3]. It has excellent biocompatibility, low solubility, strong adsorption, and high osteoinductive and osteoconductive properties, enabling it to be a suitable biomaterial for bone and dental filling, and metallic implant coating [4-9]. This makes much research regarding Hap [10-15]. However, HAp is inactive against pathogenic microorganisms that can infect bone tissue and cause complications [16,17]. Therefore, there is a need to develop HAp-based drug delivery systems (DDS) that can release biologically active compounds locally and controllably to treat bone infections [18-20].

One possible way to achieve this matter is by substituting the hydroxyl OH^- ions in the apatitic network with oxygenated species, such as peroxide ions and molecular oxygen. These species have oxidizing properties that can protect living beings against infections by producing reactive oxygen intermediates (ROI) or by increasing the local oxygen partial pressure [21-29]. Moreover, they can be naturally eliminated by specific enzymes, such as superoxide dismutases and peroxidases that regulate their overall activity

* Corresponding author.
Email: nandiyanto@upi.edu
https://doi.org/10.21924/cst.9.1.2024.1385

and ensure the antioxidant effects. However, the synthesis and characterization of oxygen-doped HAp have not get much attention in the literature, and the effect of the calcium-to-phosphorus ratio (Ca/P) on their physicochemical properties is still unclear. Over the years, the synthesis of oxygenated apatite (OA) has been explored in various studies, each method of which offers its advantages and nuances. Several examples are in the following:

(i) Some researchers prepared OA crystallized under the physiological conditions (i.e. 37°C and pH 7.40) by the reaction and precipitation of phosphate and calcium solutions. The calcium solution was get by dissolving calcium salt $CaCl_2$ in hydrogen peroxide (30%) solution. The phosphate solution was prepared by adding phosphoric acid into a solution containing oxygenated water (30%) [23].

(ii) Some researchers synthesized OA from the hydrolysis of cured brushite cement in aqueous medium. Then, they obtained an apatite containing both molecular oxygen and peroxide ions, which could be removed by heating (300°C) the final product [30].

(iii) Some researchers studied the effect of the Ca/P ratio on the chemical and structural properties of oxygenated apatite synthesized by neutralization [31].

(iv) Some researchers developed OA by controlling the hydrolysis of dicalcium phosphate dihydrate or brushite with oxygenated water. They resulted a non-stoichiometric apatite matrix with advantageous properties [32].

The synthesis of oxygenated apatite (OA) by the double decomposition method has several advantages over other methods, such as neutralization [23,31], cement [30], and dissolution-reprecipitation [21]. The double decomposition method is simple, fast, and low-cost, and it allows the control of the Ca/P ratio and the pH of the solution. Moreover, this method produces OA with high purity and a uniform particle size distribution, which are desirable for biomedical applications [25,27].

The Ca/P ratio is an important parameter that affects the chemical and structural composition of OA. This ratio determines the type and the amount of oxygenated species that are incorporated into the apatitic network. The oxygenated species can be either peroxide ions (O_2^{2-}), replacing the hydroxyl ions (OH^-), or molecular oxygen (O_2), occupying the interstitial sites in the apatitic tunnels (Fig. 1). The oxygenated species can also determine the crystallinity, morphology, and surface area of OA, which in turn affect its physicochemical and biological properties [21,23].

The antibacterial activity of OA is mainly attributed to the release of molecular oxygen and peroxide ions from the apatitic structure. These species can create oxidative stress that can damage the cell membrane, DNA, and proteins of the bacteria, leading to their death. The antibacterial activity of OA can be evaluated by measuring the oxygen partial pressure and the peroxide ion concentration in the solution, as well as by counting the number of viable bacteria after exposure to OA. The antibacterial activity of OA can be enhanced by optimizing the Ca/P ratio and the synthesis conditions [16,21,28].

This paper presented a novel phosphocalcic biomaterial with an apatitic structure. The product contained oxygenated species at oxidation degrees greater than or equal to –2 in the apatitic tunnels. The chemical formula of this biomaterial was $Ca_{10}(PO_4)_6(OH)_2O_2$. We synthesized OA by the double decomposition method, which involved precipitating calcium nitrate and diammonium phosphate solutions in an ammonia buffer. We varied the Ca/P ratio and analyzed the resulting products by means of infrared absorption spectroscopy (FTIR), X-ray diffraction (XRD), thermal analysis (TG-DTA), nitrogen adsorption-desorption (BET), and elemental chemical analysis. We also investigated how the Ca/P ratio affects the crystallinity, morphology, surface area, and oxygen content of OA. We furthermore evaluated the antibacterial activity of OA against anaerobic bacteria by measuring the oxygen partial pressure and the peroxide ion concentration. We here demonstrated that OA is a promising biomaterial for bone infection prevention and treatment.

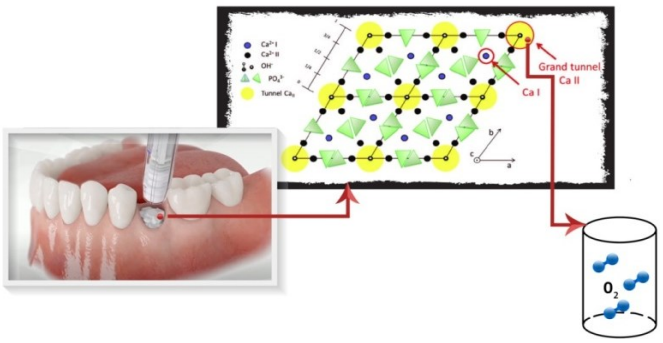

Fig. 1. Explanatory schematic image of the insertion of molecular oxygen into apatitic tunnels for dental filling

2. Materials and Methods

2.1. Preparation of OA samples

We prepared OA with various Ca/P ratios by the double decomposition method. This method involved two solutions: calcium nitrate ($Ca(NO_3)_2$,$4H_2O$/10% H_2O_2) and diammonium phosphate ($(NH_4)_2HPO_4$/10% H_2O_2), as well as an ammonia solution to adjust the pH (Fig. 2). We heated the calcium nitrate solution to boiling and added the ammonia solution dropwise until we get pH of about 10.5. This is the condition for OA formation. Then, we added the diammonium phosphate solution dropwise while maintaining the pH with ammonia. The initial Ca/P ratios were 1.67, 1.65, 1.63, 1.6 and 1.57. We boiled the suspension for 30 min, and filtered it while hot and dried it at 80°C. The products had a light-yellow color. We then heated them at 300°C for two hours to convert the peroxide ions to molecular oxygen. The final products had a white color, containing molecular oxygen in the apatitic lattice due to the dismutation of the peroxide ions. We obtained all chemicals from Sigma Aldrich (Westphalia, Germany), and all chemicals were used directly as received.

2.2. Product characterization

To support the analysis, several characterizations were

done, including FTIR (Shimadzu FT-IR 8400S series instrument (SHIMADZU, Duisburg, Germany), XRD (a Shimadzu (XRD Shimadzu 6000) diffractometer with Cu-Kα radiation (1.5418 A˚)), TG-DTA (Shimadzu DTG-60 simultaneous DTA-TG apparatus with a heating rate of 10°C/min and heated in the range of 25 to 1000°C), nitrogen adsorption-desorption, and elemental chemical analysis. Detailed information regarding these analyses is explained elsewhere [33-39]. In the FTIR analysis, the pellets were prepared by mixing 1 mg of powder with 200 mg of spectroscopic grade (KBr) and recorded the FTIR spectra in the range of 400–4000 cm^{-1}.

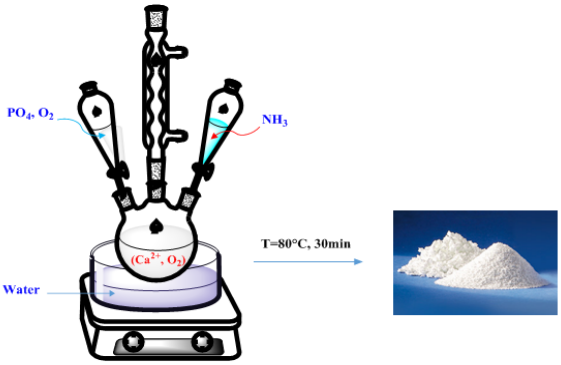

Fig. 2. Preparation of oxygenated apatite using double decomposition reaction

We determined the molar Ca/P ratio by the inductively coupled plasma atomic emission spectroscopy (ICP–AES) method, which involved nebulizing and drying the liquid sample under an argon flow and atomizing it in the plasma torch. In this case, reference solutions with a background salt for the concentration calibration were used.

We measured the specific surface area by BET (Brunaur-Emmett-Teller) and BJH (Barret-Joyner-Halenda) methods using an Autosorb 1 instrument. Furthermore, the samples under a secondary vacuum for 12 h at 70°C was degassed. We used nitrogen gas with a molecular mass of 28,013 g, a cross-section of 16,200 A^2, and a liquid density of 0.808 g/cc. We performed the measurements at 77 K and quantified the molecular oxygen in the OA by volumetry. Then, 6 ml of perchloric acid from the bromine bulb to 0.5 g of OA in the flask were added to release molecular oxygen and carbon dioxide from the apatite tunnel. We measured the volume of molecular oxygen using a mercury-filled U-tube and trapped the carbon dioxide in the sodium hydroxide solution and then titrated it with hydrochloric acid to calculate the number of moles of carbon dioxide in the OA [40].

3. Results and Discussion

3.1. FTIR spectroscopy

To analysis the chemical structure in the sample, FTIR analysis was done. Detailed information regarding FTIR is explained elsewhere [41-43].

FTIR was used to analyze the OA samples with various Ca/P ratios (1.67, 1.65, 1.63, 1.6, and 1.57). Then, we obtained data from the reaction medium. We then identified the IR absorption bands corresponding to the deformations and elongations of the groups and ions in the phosphate (Fig. 3). The FTIR spectra showed the typical absorption bands of phosphate groups (PO_4^{3-}) in OA at wavenumber of 566, 603, 961, and 1036 cm^{-1} [44]. The vibrational band at wave number near 1420 cm^{-1} for pure OA represented carbonate ions (CO_3^{2-}). It indicates for the sample to be carbonated OA [45]. Meanwhile, the large absorption band between 2600 and 3800 cm^{-1} and the small band at 1630 cm^{-1} represented the existence of water molecules in the samples [46]. The analysis showed that the products were highly pure without containing any intermediate phase due to the controlled pH of the solution during the reaction. The reaction was fast in view of the high reaction temperature (80°C). However, the carbon dioxide in the solution resulted in the formation of a slightly carbonated OA.

Fig. 4 and Fig. 5 successively show the IR absorption bands of the ions PO_4^{3-} and HPO_4^{2-} in the synthesized oxygenated apatitic products. The intensities relating to the phosphate ion bands increased with the increases in the Ca/P ratio, while the intensity of the hydrogen phosphate ion bands decreased with the increases in Ca/P ratio.

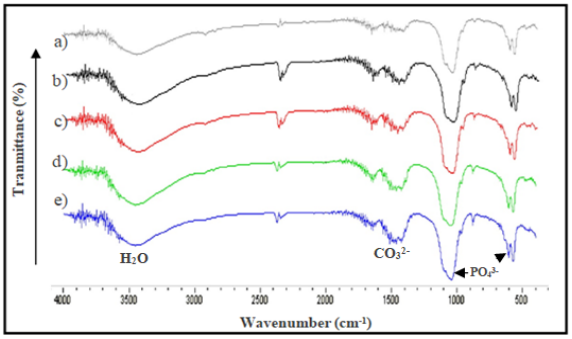

Fig. 3. Absorption FTIR spectra of the reaction products of the various Ca/P ratios (a: 1.57, b: 1.67, c: 1.65, d: 1.63, and e: 1.6)

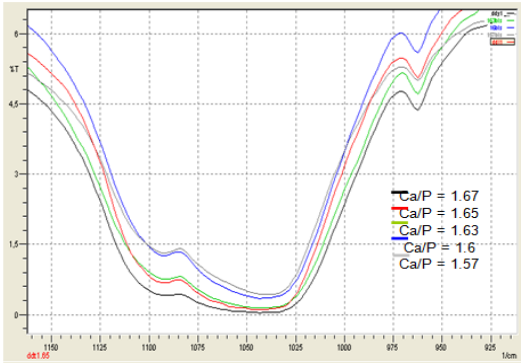

Fig. 4. Changes in the absorption bands (PO_4^{3-}) with various Ca/P ratios.

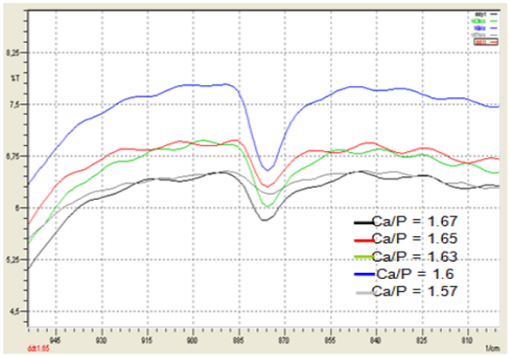

Fig. 5. Changes in the absorption bands (HPO_4^{2-}) with various Ca/P ratios

3.2. X-ray diffraction characterization

To understand the structure of the product, we used XRD analysis. Detailed information regarding XRD is explained elsewhere [47].

We examined the XRD diagrams of apatitic products with various Ca/P ratios of 1.67, 1.63, and 1.57. We obtained data from the reaction medium. The products at room temperature were then prepared and calcined at 300°C. The diagrams showed the formation of a poorly crystallized apatitic phase with broad, diffuse lines (Fig. 6). The XRD patterns showed the characteristic diffraction planes of a poorly crystallized hydroxyapatite in the hexagonal crystal system (JCPDS # 09-0432) [48]. Fig. 7 meanwhile shows the XRD spectra of reaction products with three various Ca/P ratios of 1.67, 1.63, and 1.57, calcined at 900°C. XRD analysis revealed that the product with Ca/P ratio = 1.67 became a pure, well-crystallized phosphocalcic hydroxyapatite phase with very fine lines suggesting that no other crystalline phase was present. We also found for the formation of a new phase of tricalcium phosphate (β-TCP). It seemed to be mixed with the apatite. The intensity proportion of β-TCP increased when we decreased the Ca/P ratio. The β-TCP phase resulted from the thermal decomposition of a non-stoichiometric phosphocalcic oxygenated apatite and it existed at low temperatures [49].

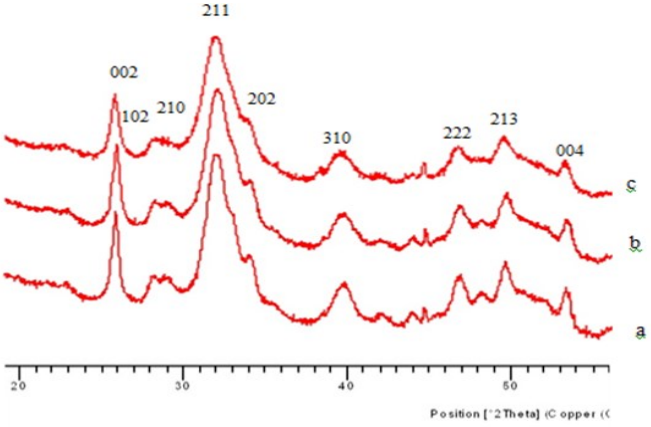

Fig. 6. XRD of the OA samples with various Ca/P ratios calcined at 300°C (a:1.67, b: 1.63, and c: 1.57)

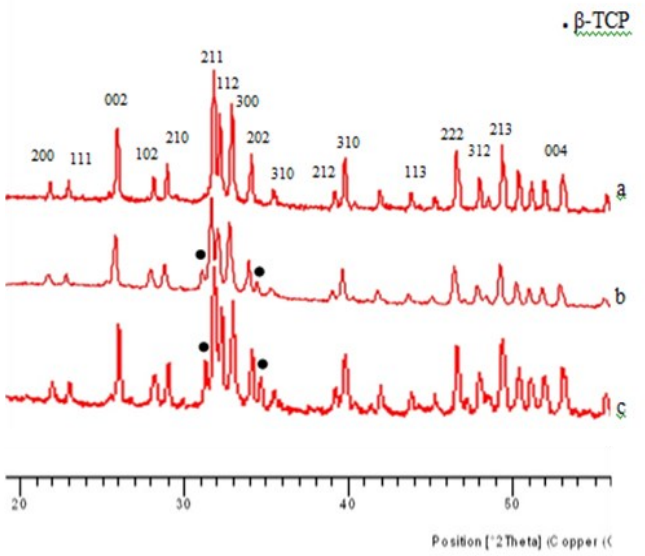

Fig. 7. XRD of the OA samples with various Ca/P ratios calcined at 900°C (a:1.67, b: 1.63, and c: 1.57)

3.3. Thermogravimetric evaluation and differential thermal analysis

To analysis effect of temperature on the performance of the sample, TG-DTA analysis was done. Detailed information regarding TG-DTA is explained elsewhere [50].

TGA and DTA were used to measure the mass loss and the thermal variations of the OA (Ca/P = 1.67) that we prepared from room temperature to 1000°C under nitrogen flow with a heating rate of 10°C/min. The TGA curve (Fig. 8) showed two small mass losses at the beginning of the heating process and 600°C. The first mass loss was due to desorption of water molecules, in which this water adsorbed on the surface of oxygenated apatite and was not bound to their crystal structure. The second one was due to the removal of residual carbonates of type A. We identified the detection at around 1450 cm^{-1} [51-53].

The literature describes the possibility of substituting the hydroxyl ions OH^- (hydroxyapatite of the A-type) and/or the phosphate groups PO_4^{3-} (hydroxyapatite of the B type) with the carbonate ions CO_3^{2-} [54, 55]. The DTA curve for oxygenated porous apatite (Fig. 8) showed the presence of two exothermic effects occurred at temperatures close to 50°C and beyond 450°C, which corresponded to the elimination of the water molecules adsorbed on the surface of this material and the elimination of the carbonate ions [56]. We observed the same analysis results for the other Ca/P ratios. This confirms the fact that the prepared apatites were thermally stable.

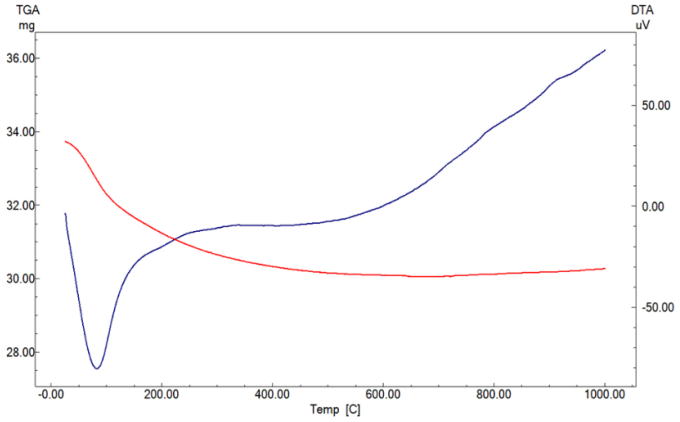

Fig. 8. Thermogravimetric and differential thermal analysis of OA-Ca/P=1.67.

Table 1. Calcium, phosphorus, and measured Ca/P ratio of the OA samples with different experimental Ca/P ratios.

Sample	Ca (mg/L)	P (mg/L)	Ca/P
Ca/P = 1.67 + 10% H_2O_2	336.8	154.5	1.68
Ca/P = 1.65 + 10% H_2O_2	332.01	153.2	1.67
Ca/P = 1.63 + 10% H_2O_2	339.6	158.6	1.65
Ca/P = 1.60 + 10% H_2O_2	345	164.1	1.62
Ca/P = 1.57 + 10% H_2O_2	338.12	162.8	1.60

3.4. Chemical analysis

Table 1 presents the summary of the chemical analysis

results. It shows that the measured Ca/P atomic ratios agreed well with the Ca/P ratios we initially introduced. When the Ca/P ratio decreased from 1.68 to 1.60, we moved away from stoichiometry. This variation in the Ca/P ratio could explain the formation of non-stoichiometric apatitic phases presenting calcium defects.

3.5. Isotherms adsorption

We evaluated the effect of molecular oxygen on the specific surface area, pore volume, and pore size of the precipitated samples. Here, the BET theory method was used to study the texture of the samples and determine their surface area, and the BJH desorption method to understand the total pore volume in the sample [57]. Detailed information regarding surface area is explained elsewhere [58].

Fig. 9 shows the analysis results gained from nitrogen isotherms for N_2 adsorption-desorption on the prepared OA samples with various ratios. The isotherms showed a gradual increase in the amount adsorbed with the relative equilibrium pressure for values of P/P_0 higher than 0.6. At low pressure, adsorption is stronger in the micropores due to the strong interaction gas-solid. The desorption process was not reversible, and showed a hysteresis of desorption relative to adsorption. The isotherm was of type IV according to the IUPAC classification, typical of adsorption in the mesopores [58]. The existence of hysteresis suggested the presence of mesoporosity on the surface of the oxygenated apatite studied, which produced capillary condensation. Table 2 presents the summary of the results of the measurements of specific surface, pore volume, and average pore diameter of the OA samples prepared with different ratios.

The analysis showed that the specific surface area did not change with the Ca/P ratio and ranged between 98 and 102 m^2/g.

3.6. Effect of ratio Ca/P on molecular oxygen content

Table 3 shows the Ca/P ratio, the molecular oxygen content, and the chemical formula of the phosphocalcic OA for various Ca/P ratios. The curve (Fig. 10) shows how the molecular oxygen content changes with the Ca/P ratio.

The curve had two parts:

(i) The first part showed an increase in the molecular oxygen content as the Ca/P ratio increased, reaching the maximum value of 2.3% at Ca/P = 1.65 with the chemical formula of $Ca_{9,9}(PO_4)_6(OH)_{1,25}(O_2)_{0,74}(CO_3)_{0,01}$. This may be explained by the formation of apatitic tunnels. The level of molecular oxygen in oxygenated apatite decreases when the Ca/P atomic ratio decreases. This could be due to the formation of apatitic tricalcium phosphate, to the detriment of the formation of apatitic tunnels, which could trap molecular oxygen. The formation of these tunnels was disadvantaged.

(ii) The second part showed a constant molecular oxygen content for higher Ca/P ratios.

For comparison, some researchers prepared an oxygenated apatite with a Ca/P ratio and chemical formula $Ca_{9.59}(PO_4)_{5.82}(HPO_4)_{0.18}(OH)_{0.74}(O_2^{2-})_{0.31}(O_2)_{0.45}$ [23]. Also, some researchers synthesized OA from the hydrolysis of cured brushite cement in an aqueous medium with a molecular oxygen content of 3% [21]. Some researchers synthesized an oxygenated apatite by neutralization and obtained a molecular oxygen content of 2.24%, and a chemical formula of $Ca_{9,9}(PO_4)_6(OH)_2(O_2)_{0,69}(CO_2)_{0,01}$ [31].

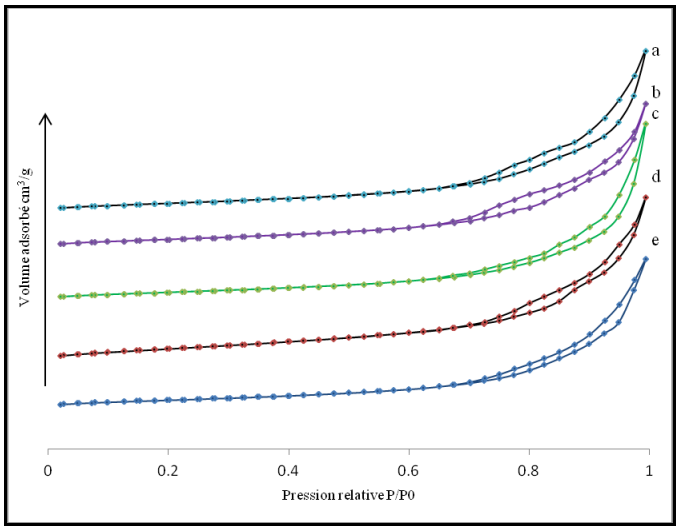

Fig. 9. Adsorption-desorption isotherms of N_2 on OA samples with various Ca/P ratios calcined at 300°C (a: 1.57, b: 1.60, c: 1.63, d: 1.65, and e:1.67).

Table 2. Volumetric analysis of the oxygenated apatite samples with various Ca/P ratios.

Sample	Specific surface (m^2/g)	Pore volume (cc/g)	Pore rays (A°)
Ca/P = 1.67 + 10% H_2O_2	100.2	0.472	26.37
Ca/P = 1.65 + 10% H_2O_2	98.5	0.531	31.42
Ca/P = 1.63 + 10% H_2O_2	98.0	0.434	28.23
Ca/P = 1.60 + 10% H_2O_2	100.0	0.677	25.62
Ca/P = 1.57 + 10% H_2O_2	102.6	0.642	29.82

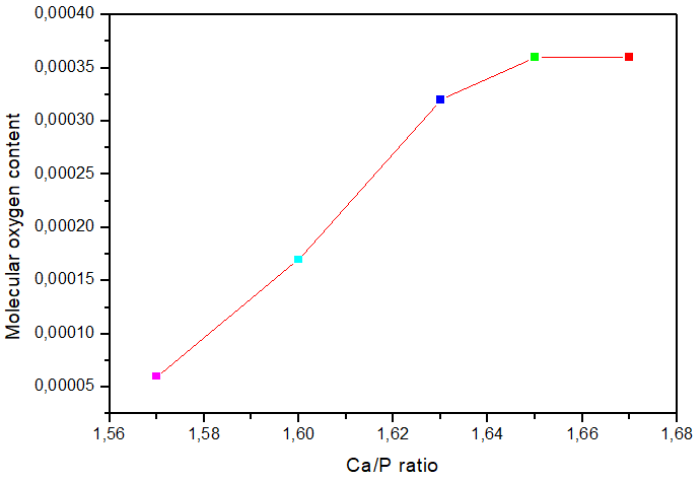

Fig. 10. Variation of the molecular oxygen content with the Ca/P ratio

Table 3. $n(O_2)$, $n(CO_2)$, and chemical formula of oxygenated apatite for various Ca/P ratios.

Ca/P ratio	$n(O_2)$ mole ($\times 10^{-4}$)	$n(CO_2)$ mole ($\times 10^{-6}$)	Chemical formula	O_2 content
1.67	3.6	6.1	$Ca_{10}(PO_4)_6(OH)_{1,25}(O_2)_{0,74}(CO_3)_{0,01}$	2.30
1.65	3.6	7.2	$Ca_{9,9}(PO_4)_6(OH)_{1,25}(O_2)_{0,74}(CO_3)_{0,01}$	2.30
1.63	3.2	6.4	$Ca_{9,78}(PO_4)_6(OH)_{1,34}(O_2)_{0,65}(CO_3)_{0,01}$	2.04
1.60	1.7	4.8	$Ca_{9,6}(PO_4)_6(OH)_{1,65}(O_2)_{0,34}(CO_3)_{0,01}$	1.07
1.57	0.6	2.2	$Ca_{9,42}(PO_4)_6(OH)_{1,88}(O_2)_{0,12}$	0.37

4. Conclusion

FTIR analysis of OA prepared with various Ca/P ratios (1.67, 1.65, 1.63, 1.6 and 1.57) showed the presence of all IR absorption bands corresponding to symmetrical and anti-symmetrical group elongations in the apatitic phase. The reticular distances corresponded well to literature values, indicating the high purity of the products synthesized. No intermediate phase was observed as the pH of the solution was controlled during the reaction. The reaction was rapid due to the high temperature (80°C). However, the CO_2 present in the solution allowed to the creation of a slightly carbonated OA. The double decomposition synthesis method was suitable for this process as it enabled the pH of the solution to be controlled throughout precipitation. The specific surface area of around 100 ± 2 m^2/g did not change with the Ca/P ratio. The amount of molecular oxygen was higher for higher Ca/P ratios.

References

1. A. Errich, K. Azzaoui, E. Mejdoubi, B. Hammouti, N. Abidi, N. Akartasse, L. Benidire, S. EL Hajjaji, R. Sabbahi, and A. Lamhamdi, *Toxic heavy metals removal using a hydroxyapatite and hydroxyethyl cellulose modified with a new Gum Arabic.* Indonesian Journal of Science and Technology, 6(1) (2021) 41-64.
2. F.S. Irwansyah, A.I. Amal, E.P. Hadisantoso, A.R. Noviyanti, D.R. Eddy, R. Risdiana, S. Suryana, and S.B. Md Zain, *How to make and characterize hydroxyapatite from eggshell using the hydrothermal method: potential insights for drug delivery system.* Indonesian Journal of Science and Technology, 8(3) (2023) 469-486.
3. Y.A. Svakhina, M.E. Titova, and Pyagay, I.N. (2023). Products of apatite-nepheline ore processing in the synthesis of low-modulus zeolites. *Indonesian Journal of Science and Technology*, *8*(1), 49-64.
4. H. A. Siddiqui, K. L. Pickering, M. R. Mucalo, *A Review on the Use of Hydroxyapatite-Carbonaceous Structure Composites in Bone Replacement Materials for Strengthening Purposes*, Materials (Basel). (2018) 11(10) 1813.
5. E. Fiume, G. Magnaterra, A. Rahdar, E. Verne, F. Biano, *Hydroxyapatite for biomedical applications: a short overview*, Ceramics, 4, (2021) 542-563.
6. F. R. Maia, V. M. Correlo, J. M. Oliveira, R. L. Reis, *Natural Origin Materials for Bone Tissue Engineering: Properties, Processing, and Performance*, Principles of Regenerative Medicine (III), (2019) 535- 558 (32).
7. S. V. Dorozhkin, *Dental applications of calcium orthophosphates (CaPO4)*, J. Dent. Res. (2019), 1 (2) 1007
8. N. Akartasse, et al., *Natural product-based composite for extraction of arsenic (III) from wastewater*, Chemistry Central Journal. 11 (2017) Article 33.
9. A. D. N'diaye, M. S. A. Kankou, B. Hammouti, A. B. D. Nandiyanto, D. F. Al Husaeni, *A review of biomaterial as an adsorbent: From the bibliometric literature review, the definition of dyes and adsorbent, the adsorption phenomena and isotherm models, factors affecting the adsorption process, to the use of typha species waste as a low-cost adsorbent,* Communications in Science and Technology (2022), 7(2), 140–153
10. S. Herradi, I. Adouar, M. Zerrouk, S. Bouhazma, M. E. Omari, R. Ouarsal, M. Khaldi, B. El Bali, & M. Lachkar, *Physicochemical study of magnesium zinc codoped-hydroxyapatite.* Moroccan Journal of Chemistry, 12(3) (2024) 1240-1253.
11. S. Latifi, S. Saoiabi, E. H. Loukili, K. Azzaoui, B. Hammouti, G. Hanbali, S. Jodeh, R. Sabbahi, A. Saoiabi, *Preparation of cellulose-hydroxyapatite composites using 3D printing for biomedical applications.* Moroccan Journal of Chemistry, 12(2) (2024) 884-914.
12. F. Hosseini, F. Soltanolkottabi, M. M. Behrouzfar, & H. Jafari, *Powder mixture of hydroxyapatite and tetracalcium phosphate for hard tissue applications.* Moroccan Journal of Chemistry, 12(2), (2024) 534-553.
13. S. Herradi, M. Zerrouk, A. Bouayad, R. Ouarsal, M. Khaldi, B. El Bali, & M. Lachkar, *Removal of methylene blue with a highly effective hydroxyapatite-silica nanocomposite.* Moroccan Journal of Chemistry, 12(1) (2024) 267-285.
14. L. El Hammari, S. Latifi, S. Saoiabi, K. Azzaoui, B. Hammouti, A. Chetouani, & R. Sabbahi, *Toxic heavy metals removal from river water using a porous phospho-calcic hydroxyapatite.* Moroccan Journal of Chemistry, 10(1) (2022) 62-72.
15. D.H. Siswanto, A.S. Aminatun, *Molarity optimization of calcium hydroxide in the forming of bioceramic hydroxyapatite from nano coral by precipitation method.* Moroccan Journal of Chemistry, 8(1) (2020) 24-31
16. R. Ghosh, S. Das, S. P. Mallick, Z. Beyene, *A review on the antimicrobial and antibiofilm activity of doped hydroxyapatite and its composites for biomedical applications,* materialstoday communications, (2022), 31, 103311.
17. N. Akartasse, et al., *Environmental-Friendly Adsorbent Composite Based on Hydroxyapatite/Hydroxypropyl Methylcellulose for Removal of Cationic Dyes from an Aqueous Solution*. Polymers, (2022), 11(14) 2147
18. S. Lara-Ochoa, W. Ortega-Lara, C. E. Guerrero-Beltrán, *Hydroxyapatite nanoparticles in drug delivery: physicochemistry and applications*, Pharmaceutics (2021) 13 (10) 1642.
19. S. Jerdioui, et al., *Effects of gallic acid on the nanocrystalline hydroxyapatite formation using the neutralization process*, Journal of Trace Elements and Minerals, (2022) 2773-0506.
20. M. U. Munir, et al., *Nanohydroxyapatite as a delivery system: overview and advancements*, Artif. Cells Nanomed. Biotechnol. (2021) 49 (1), 717–727.
21. S. C. Oh, Y. Lei, H. Chen, D. Liu, *Catalytic consequences of cation and anion substitutions on rate and mechanism of oxidative coupling of methane over hydroxyapatite catalysts,* Fuel, 191 (2017) 472-485.
22. L. Naanaai, K. Azzaoui, E. Mejdoubi, A. Lamhamdi, M. Lakrat, S. Jodeh, *Study and Optimization of Oxygenated Apatite Obtained by Dissolution-Reprecipitation of Hydroxyapatite in a Solution of Hydrogen Peroxide,* Chemistry Africa.3, (2019), 227–235,
23. S. Belouafa, H. Chaair, H. Loukili, K. Digua, B. Sallek, *Characterization of Antiseptic Apatite Powders Prepared at Biomimetics Temperature and pH*, Materials Research (2008), 11, No. 1, 93-96.
24. R. Vona, L. Pallotta, M. Cappelletti, C. Severi, P. Matarrese, *The Impact of Oxidative Stress in Human Pathology: Focus on Gastrointestinal Disorders*, Antioxidants, 10(2) (2021) 201
25. E. Tvrdá, F. Benko, M. Ďuračka, *Oxidative Stress as an Underlying Mechanism of Bacteria-Inflicted Damage to Male Gametes,* Oxygen, *2*(4) (2022) 547-569*;*
26. J. P. Taylor, H. M. Tse, *The role of NADPH oxidases in infectious and inflammatory diseases, Redox Biology*, 48 (2021) 102159.
27. J. Pravda, *Hydrogen peroxide and disease: towards a unified system of pathogenesis and therapeutics, Molecular Medicine,* 26 (2020) 41.
28. E. B. Kurutas, *The importance of antioxidants which play the role in cellular response against oxidative/nitrosative stress: current state*, Nutrition journal, 15 (2016) 71.

29. A. Sangpanya, B. Uea-aranchot, C. Rakkhansaeng, U. Tapsuri, M. Tanapoomchai, A, Teerakapong, Effect of Hydroxyl Radical from Blue Light and Hydrogen Peroxide on Porphyromonas gingivalis in Biofilms, (Khon Kaen Dent J, 21 No.1(2018),
30. R. Yahyaoui, E. Mejdoubi, K. Azzaoui, A. Lamhamdi, S. Elabed, B. Hammouti, *Preparation of oxygenated apatite from hydrolysis of cured brushite cement in aqueous medium,* (2014). Der Pharma Chemica, 6(6), 133-138
31. S. Jerdioui, L. L. Elansari, H. Bouammali, K. Azzaoui, R. Sabbahi, B. Hammouti, et al. *Effect of Calcium/phosphorus Ratio on the Chemical and Structural Properties of Oxygenated Apatite Synthesized by Neutralization,* Mor. J. Chem., 12 (1) (2024) 145-156
32. A. Lamhamdi, *Elaboration of new phosphate matrices for odontological, environmental and industrial in using the maturation controlled and techniques of hydrolysis*, Doctoral thesis, (2013), Mohammed I University, Morocco.
33. S. Fatimah, R. Ragadhita, D.F. Al Husaeni, A.B.D. Nandiyanto, *How to calculate crystallite size from x-ray diffraction (XRD) using scherrer method.* ASEAN Journal of Science and Engineering, 2(1) (2022) 65-76.
34. A.B.D. Nandiyanto, R. Oktiani, and R. Ragadhita, *How to read and interpret FTIR spectroscope of organic material.* Indonesian Journal of Science and Technology, 4(1) (2019) 97-118.
35. A.B.D. Nandiyanto, R. Ragadhita, and M. Fiandini, *Interpretation of Fourier Transform Infrared Spectra (FTIR): A practical approach in the polymer/plastic thermal decomposition.* Indonesian Journal of Science and Technology, 8(1) (2023) 113-126
36. S. Sukamto, and A. Rahmat, *Evaluation of FTIR, macro and micronutrients of compost from black soldier fly residual: In context of its use as fertilizer.* ASEAN Journal of Science and Engineering, 3(1) (2023) 21-30.
37. E.N. Obinna, *Physicochemical properties of human hair using Fourier Transform Infra-Red (FTIR) and Scanning Electron Microscope (SEM).* ASEAN Journal for Science and Engineering in Materials, 1(2) (2022) 71-74.
38. R. Ragadhita, and A.B.D. Nandiyanto, *Why 200°C is effective for creating carbon from organic waste (from thermal gravity (TG-DTA) perspective)?* ASEAN Journal for Science and Engineering in Materials, 2(2) (2023) 75-80.
39. F.S. Irwansyah, A.I. Amal, E.W. Diyanthi, E.P. Hadisantoso, A.R. Noviyanti, D.R. Eddy, and R. Risdiana. *How to read and determine the specific surface area of inorganic materials using the Brunauer-Emmett-Teller (BET) method.* ASEAN Journal of Science and Engineering, 4(1) (2024) 61-70.
40. M. Jarcho*, Calcium phosphate ceramics as hard tissue prosthetics*, Clin. Orthop. Relat. Res. 157 (1981) 259-78
41. A.B.D. Nandiyanto, R. Ragadhita, and M. Fiandini, *Interpretation of Fourier Transform Infrared Spectra (FTIR): A practical approach in the polymer/plastic thermal decomposition.* Indonesian Journal of Science and Technology, 8(1) (2023) 113-126
42. Sukamto, S., and Rahmat, A. (2023). Evaluation of FTIR, macro and micronutrients of compost from black soldier fly residual: In context of its use as fertilizer. *ASEAN Journal of Science and Engineering*, *3*(1), 21-30.
43. E.N. Obinna, *Physicochemical properties of human hair using Fourier Transform Infra-Red (FTIR) and Scanning Electron Microscope (SEM).* ASEAN Journal for Science and Engineering in Materials, 1(2) (2022) 71-74.
44. K. Azzaoui, et al., *Synthesis of β-Tricalcium Phosphate/PEG 6000 Composite by Novel Dissolution/Precipitation Method: Optimization of the Adsorption Process Using a Factorial Design—DFT and Molecular Dynamic*. Arabian Journal for Science and Engineering, 49(1) (2024) 711–732
45. K. Azzaoui, *Preparation of hydroxyapatite biobased microcomposite film for selective removal of toxic dyes from wastewater*, Polymer 1(27) (2019) 28.
46. M. Aaddouz, et al., *Removal of methylene blue from aqueous solution by adsorption onto hydroxyapatite nanoparticles,* Journal of Molecular Structure, 1288 (2023) 135807.
47. S. Fatimah, R. Ragadhita, D.F. Al Husaeni, and A.B.D. Nandiyanto, *How to calculate crystallite size from x-ray diffraction (XRD) using scherrer method.* ASEAN Journal of Science and Engineering, *2*(1) (2022) 65-76.
48. J. Vecstaudza, M. Gasik, J. Locs, *Amorphous calcium phosphate materials: Formation, structure and thermal behaviour*, Journal of the European Ceramic Society, 39(4) (2019) 642-1649
49. A. Mokhtari, H. Belhouchet, A. Guermat*, In situ high-temperature X-ray diffraction, FT-IR and thermal analysis studies of the reaction between natural hydroxyapatite and aluminum powder,* Journal of Thermal Analysis and Calorimetry, 136 (2019) 1515–1526
50. R., Ragadhita, and A.B.D. Nandiyanto, (2023). Why 200°C is effective for creating carbon from organic waste (from thermal gravity (TG-DTA) perspective)? *ASEAN Journal for Science and Engineering in Materials*, *2*(2), 75-80.
51. L. Simkova, P. Sulcova, *Characterization and thermal behavior of hydroxyapatite prepared by precipitation*, Journal of Thermal Analysis and Calorimetry, 138 (2019) 321–329
52. S. G. Choi, S. S. Park, S. Wu, J. Chu, *Methods for calcium carbonate content measurement of biocemented soils*, J. Mater. Civ. Eng. 29 (11) (2017) 06017015.
53. W. Kong, K. Zhao, C. Gao, P. Zhu, *Synthesis and characterization of carbonated hydroxyapatite with layered structure*, Materials Letters**,** 255 **(**2019) 126552
54. B. Wang, Z. Zhang, H. Pan, *Bone Apatite Nanocrystal: Crystalline Structure, Chemical Composition, and Architecture*, Biomimetics, (2023) 8, 90.
55. E. Skwarek, O. Goncharuk, D. Sternik, W. Janusz, K. Gdula and V. M. Gunko, *Synthesis, Structural, and Adsorption Properties and Thermal Stability of Nanohydroxyapatite/Polysaccharide Composites*, Nanoscale Research Letters, 12 (2017) 155
56. T. Virtanen, G. Rudolph, A. Lopatina, B. Al-Rudainy, H. Schagerlöf, L. Puro, et al., *Analysis of membrane fouling by Brunauer-Emmett-Teller nitrogen adsorption/desorption technique*, Sci Rep. 10 (2020) 3427.
57. F. Sotomayor, K. A. Cychosz, M. Thommes, *Characterization of Micro/Mesoporous Materials by Physisorption: Concepts and Case Studies*, Acc. Mater. Surf. Res. 3(2) (2018) 34-50.
58. F.S., Irwansyah, A.I., Amal, E.W., Diyanthi, Hadisantoso, E.P., Noviyanti, A.R., Eddy, D.R., and R. Risdiana, *How to read and determine the specific surface area of inorganic materials using the Brunauer-Emmett-Teller (BET) method.* ASEAN Journal of Science and Engineering, 4(1) (2024) 61-70.